

Article

Photochromic Textiles Based upon Aqueous Blends of Oxygen-Deficient WO_{3-x} and TiO_2 Nanocrystals

Roberto Giannuzzi ^{1,2}, Vitantonio Primiceri ^{1,2}, Riccardo Scarfiello ^{1,*} , Marco Pugliese ¹ , Fabrizio Mariano ¹, Antonio Maggiore ¹ , Carmela Tania Prontera ^{1,3,*}, Sonia Carallo ¹, Cristian De Vito ¹, Luigi Carbone ¹  and Vincenzo Maiorano ¹

- ¹ CNR NANOTEC—Institute of Nanotechnology c/o Campus Ecotekne, University of Salento, Via Monteroni, 73100 Lecce, Italy; roberto.giannuzzi@nanotec.cnr.it (R.G.); vitantonio.primiceri@unisalento.it (V.P.); marco.pugliese@nanotec.cnr.it (M.P.); fabrizio.mariano79@gmail.com (F.M.); antonio.maggiore@nanotec.cnr.it (A.M.); sonia.carallo@nano.cnr.it (S.C.); cristian.devito@nanotec.cnr.it (C.D.V.); luigi.carbone@nanotec.cnr.it (L.C.); vincenzo.maiorano@nanotec.cnr.it (V.M.)
- ² Department of Mathematics and Physics “Ennio De Giorgi”, University of Salento, 73100 Lecce, Italy
- ³ Istituto per la Microelettronica e Microsistemi (IMM)—CNR, Via Monteroni, 73100 Lecce, Italy
- * Correspondence: riccardo.scarfiello@nanotec.cnr.it (R.S.); tania.prontera@nanotec.cnr.it (C.T.P.)

Abstract: With the main objective being to develop photochromic smart textiles, in this paper, we studied the photochromic behavior of WO_{3-x} nanocrystals (NCs) cooperatively interacting with variable amounts of TiO_2 NCs. We tested several blends of $WO_{3-x}:TiO_2$ NCs, admixed in different compositions (relative molar ratio of 4:0, 3:1, 2:2, 1:3, 0:4) and electrostatically interfacing because of opposite values of Z-potential, for photo-induced chromogenic textiles. We further monitored the photochromic sensitivity of NC-impregnated textiles after exposure to a few solvents (i.e., methanol, ethanol, and isopropanol) or when over-coated with different polymeric matrices such as natural cellulose or ionic conductive Nafion. The optimization of the compositions of the $WO_{3-x}:TiO_2$ blends embedded in polymeric matrices, allowed the nanostructured photochromic textiles to show rapid and tunable coloration (<5 min) and bleaching kinetics (~5 in at 75 °C or 6 h at room temperature) along with good recovery and cycling stability. This study features a simple strategy for the widespread application of $WO_{3-x}:TiO_2$ -based photochromic smart textiles.

Keywords: smart textile; photochromism; inorganic nanoparticles



Citation: Giannuzzi, R.; Primiceri, V.; Scarfiello, R.; Pugliese, M.; Mariano, F.; Maggiore, A.; Prontera, C.T.; Carallo, S.; De Vito, C.; Carbone, L.; et al. Photochromic Textiles Based upon Aqueous Blends of Oxygen-Deficient WO_{3-x} and TiO_2 Nanocrystals. *Textiles* **2022**, *2*, 382–394. <https://doi.org/10.3390/textiles2030021>

Academic Editor: Laurent Dufosé

Received: 28 April 2022

Accepted: 17 June 2022

Published: 1 July 2022

Publisher’s Note: MDPI stays neutral with regard to jurisdictional claims in published maps and institutional affiliations.



Copyright: © 2022 by the authors. Licensee MDPI, Basel, Switzerland. This article is an open access article distributed under the terms and conditions of the Creative Commons Attribution (CC BY) license (<https://creativecommons.org/licenses/by/4.0/>).

1. Introduction

The term ‘smart textiles’ is used to describe those fabrics that, thanks to the integration of specific digital tools, devices, and sensors, show supplementary features which make them sensitive to environmental conditions and/or able to interact with the end-user [1–5]. These technologies are recently receiving growing interest for extensive applications in different fields spanning from the safety industry to the healthcare and fashion industry [6]. A specific class of materials used for the fabrication of smart textiles is chromogenic materials, whereby the change of their color is reversibly induced as a response to an environmental stimulus, which can be thermal, optical, mechanical, electrical, etc. [7]. In particular, photochromism is a photo-induced modification of the electronic state of the material and it is a phenomenon already used in various commercial products such as sunglasses, packaging, cosmetics, memories, sensors, and displays [8]. Thus, we saw a potential interest for textile applications to open perspectives towards the development of UV protective and sensing clothes that can find considerable implications in the safety and military industries [7,9,10]. Disparate examples of photochromic fabrics were obtained by using several organic dyes, such as spirooxazines, spiropyrans and naphthopyrans, employed with different kinds of integration processes [11–18]. Traditional and innovative

dyeing techniques based on supercritical CO₂ were used for the production of photochromic textiles by using organic molecules [16,17]. An alternative approach is based on electrospinning, Zheng et al. reported electrospun polycaprolactone fibers doped with photochromic dyes and their subsequent embroidering into commercial fabrics for the development of wearable UV indicators [14]. Printing techniques such as inkjet and screen printing were also widely used for the development of photochromic textile, by incorporating the dyes into polymeric matrices to obtain printable inks [11–13]. The electrostatic layer-by-layer self-assembly method of photochromic microcapsules was also reported for the preparation of photochromic cotton fabric [15].

Despite this, organic materials are at the same time largely affected by external environmental conditions such as oxygen and pH, hence, microencapsulation processes are usually required to ensure long-time service [13,15,18]. Nevertheless, embedding photochromic dyes into a rigid polymeric matrix often reduces the molecular mobility and therefore slows down the reversible modification responsible for the photochromism in organic molecules. Immobilization of photochromic dyes onto inorganic matrices, before their combination with textiles, might partially overcome those drawbacks and possibly induce enhanced color-exchange properties, stability and comfort [19–21].

Inorganic materials represent a valid alternative to organic molecules since they usually report better stability and for that have recently been under investigation for photochromic textiles fabrication [8,22–25]. Fang et al. reported the preparation of cellulose fibers with the incorporation of hackmanite micro-particles for the development of wearable UV sensors [24]. A photochromic cellulosic fabric was also obtained by screen printing of strontium aluminate pigment and aqueous binder [8]. Photochromic properties of tungsten-based materials were also exploited for the development of smart chromogenic textiles [22,23,25,26].

Bao et al. obtained photochromic textiles by a simple hydrogen bonding self-assembly of polyacrylic acid and sodium deca-tungstate [25]. Wang et al. reported waterborne tungsten-based polyvinyl alcohol (PVA) coating by simply dipping the fiber into a mixture of Na₂WO₄ and PVA and the obtained fibers showed an instantaneous color response after UV irradiation [23]. Another approach based on dip coating was developed by Ling et al. starting from WO₃ nanomaterials and PVA, obtaining photochromic fibers with a fast and reversible color switch [22]. Electrospinning is another valid technique employed to obtain fibrous substrates and it was employed by Wei et al. to fabricate fibrous photochromic membranes starting from polyvinylpyrrolidone and WO₃ [26].

Although different specific mechanisms were proposed in the literature (tungsten bronze formation where the optical transition is associated with the intervalence-charge transfer mechanism or where absorption arises from free or trapped charge carriers) [27], the photochromic performance in tungsten-based materials is determined by the behavior of optically excited electron-hole pairs [28]. Thus, by controlling the lifetime and the optical paths of these free charge carriers, the coloration performances can be controlled. For this purpose, it was reported that the photochromic properties of tungsten oxide can be improved by mixing/coupling it with other metal oxides such as TiO₂. Nowadays, consistent experimental pieces of evidence demonstrated the advantages of mixed WO_{3-x}TiO₂ materials for photochromic applications [29–32]. Such performance enhancement can be understood by evaluating the energy levels of the two materials and the formation of a junction at the WO_{3-x}-TiO₂ interface. In other words, the enhanced photochromic response is a consequence of reduced recombination paths of photogenerated carriers which result in more electrons trapped within the bandgap of the WO_{3-x} domain, contributing to the coloration process. Additionally, for tungsten oxide-based nanocomposites, polymeric matrix encapsulation proved to be a valid strategy for influencing both coloration and bleaching processes, which depend on concentrations of proton available in the nanocomposites-polymer matrix and on the diffusion rate achievable of generated proton via hydrogen bonding into the matrix [33]. However, the stronger the interaction between tungsten oxide and the matrix is, the higher and faster the coloration process could be, and the slower

the bleaching process would be. Thus, it is a big challenge to make a proper balance and compatibility between the matrix and inorganic nanoparticles to achieve a consistent coloration process followed by rapid bleaching recovery, thus achieving a suitable compromise necessary for any specific practical application.

In this context, we used for the first time, a mixture of WO_{3-x} and TiO_2 nanomaterials to obtain photochromic textiles with improved performances compared to bare WO_{3-x} . In particular, we report a low-cost and industrially suitable procedure to functionalize common textiles, through a simple impregnation method, with nanostructured active inks obtained by mixing WO_{3-x} and TiO_2 nanocrystals. A systematic study of the effect of the addition of TiO_2 nanoparticles on the photochromic response of WO_{3-x} coating textiles was achieved by simply mixing the nanocrystal solutions of the two photoactive materials. Different photochromic performances resulted from variable compositions of photoactive inks used for textile impregnation. Moreover, the photochromic response of the $\text{WO}_{3-x}:\text{TiO}_2$ blend-coated textile was evaluated in the presence of selected organic solvent and/or embedded in polymeric matrices. Coloration kinetics, operational stability toward environmental chemicals (water and oxygen), and physical stresses of the nano-functionalized and -structured smart textile were also investigated.

2. Materials and Methods

2.1. Materials

All chemicals were used as received without further purification. The following chemicals were purchased from Sigma-Aldrich (Burlington, MA, USA): methanol (MeOH, 99.9%), ethanol (EtOH, 95%), 2-propanol (i-PrOH, 95.5%), hydroxyethylcellulose (HEC, average molecular weight: 380 kDa), starch from corn. Nafion alcoholic solution (D2021CS isopropanol-based 1100 EW at 20% *w/w*) was provided by Ion Power. Fabrics were provided by our industrial partner Klopman SRL made by cotton–polyester 50/50 blend, 270 g/m³. Water-dispersed sub-stoichiometric WO_{3-x} nanocrystals (NCs) were synthesized as reported elsewhere [34]; water-dispersible TiO_2 NCs were prepared according to a previously reported procedure, with minor changes [35]. A more detailed synthetic procedure of the latter will be exhaustively reported elsewhere. Representative TEM pictures and XRD diffraction patterns of TiO_2 and WO_{3-x} nanocrystals are reported in Figure S1a–d, respectively.

2.2. Preparation of Samples and Analysis Method

Textile samples were prepared by cutting samples as 1.0 × 2.0 cm in size. NC impregnation was performed by soaking samples in a proper blend of NC solution made by different $\text{WO}_{3-x}:\text{TiO}_2$ ratio content (relative molar compositions of 4:0, 3:1, 2:2, 1:3, 0:4 expressed in WO_{3-x} % named hereafter, 100%, 75%, 50%, 25% and 0%), for 3 s and then dried on hot plate at 80 °C for 3 min. This process was repeated 10 times for each sample to ensure an adequate loading of nanostructures. The manufacturing of textiles NC functionalization is sketched in Figure 1. The photochromic properties were evaluated by irradiating samples at 320–400 nm lamp with Bromograph MF 1030 (Nuova Delta Electronica) with different time exposure. Reflectance measurements were performed soon after UV (ultraviolet) exposure with PerkinElmer Lambda 1050 UV/Vis (visible)/NIR (near-infrared) spectrophotometer in a wavelength range between 250 nm and 1000 nm. For optical properties measurements, we evaluated a negligible transmittance (data not shown), thus we acquired reflectance (R) information that can be eventually converted into absorption (Abs) as follow $\text{Abs} = 1 - \text{R}$. For photochromic measurements with different solvents exposure, 300 μL of solvent were cast on each sample and then exposed to UV radiation. Reflectance spectrum was suddenly recorded ensuring that the textile was still wetted during the measurement. The solvent impregnation process was repeated for each exposure time investigated. Photochromic measurements with starch and HEC were performed as follows: polymers were stirred in hot distilled water (80 °C) until complete powder gelation (concentration 0.05 mg/mL) before being uniformly deposited on samples by spin coating 1 mL of solutions (2000 rpm for

60 s); then, a further step of 5 min at 80 °C was adopted to ensuring complete evaporation of water. Nafion solution was spin-coated (2000 rpm for 60 s) as received without further dilutions, and dried onto the hot plate (80 °C for 5 min). Samples were then exposed to UV irradiation at different time scales and reflectance spectra were suddenly acquired.

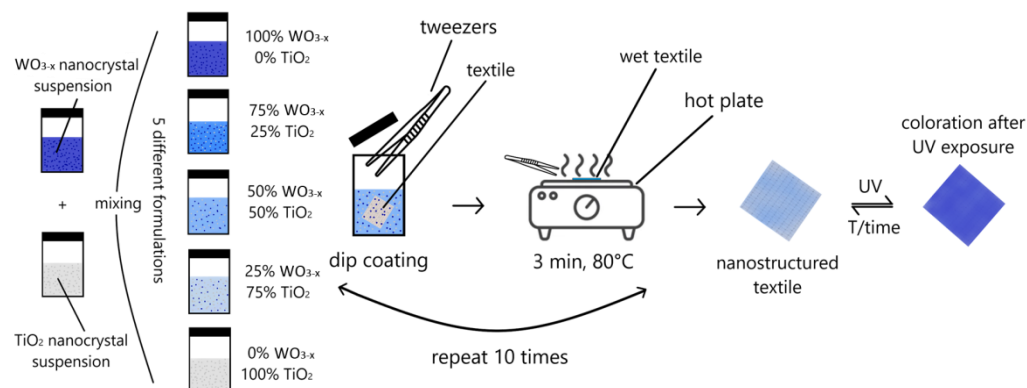


Figure 1. Schematic illustration of textile's sample functionalization with different TiO₂ and WO_{3-x} nanoparticle solution compositions.

SEM morphological investigations were carried out on NC-decorated textiles without any further treatment, with FE-SEM Zeiss Merlin (Oberkochen, Germany) equipped with a GEMINI2 column, Schottky-type electron gun and secondary electron/Inlens detectors; images were recorded at 5 kV.

TEM images of WO_{3-x} and TiO₂ nanocrystals were recorded on a JEOL JEM 1011 microscope (Peabody, MA, USA), equipped with a W filament source operating at 100 kV. Samples for TEM analysis were prepared by drop-casting a few drops of dilute nanocrystal solutions onto standard carbon-coated Cu grids, then allowing the solvent to evaporate. The as-dried sample grids were stored at 50 °C overnight before being transferred into the microscope for imaging.

XRD spectra were collected at room temperature using a Bruker D8 Discover diffractometer (Billerica, MA, USA) (operating conditions 40 kV, 40 mA) equipped with a Goebel mirror for copper radiation ($\lambda K\alpha_1 = 1.540\ 56\ \text{\AA}$, $\lambda K\alpha_2 = 1.544\ 39\ \text{\AA}$), and a scintillator detector. Samples were deposited onto a silicon zero background substrate. Data were collected in a reflection geometry at a fixed incidence angle of $\omega = 3^\circ$ while moving the detector between 5° and 120° with a step size of 0.05° .

CAM 200 (KSV Instruments Ltd., Helsinki Finland) instrument was used to allow static contact angle measurements of all the samples by the sessile drop method (water drop volume—10 μL , time between frames—16 ms).

3. Results

For the functionalization of the hydrophilic component of textiles, with the idea of defining a process extendible to various commercially available fabrics, proper water-dispersible NC solutions were adopted. In the view of industrially accessible processability, scalability, and greener chemistry, water-dispersible inorganic NC solutions of TiO₂ and WO_{3-x} were properly synthesized and processed. The chemical synthesis was performed within a hydroalcoholic environment and heated through microwave irradiation, which allows faster and in-core homogeneous heating rates. Both individual inorganic nano-components were generated without the need for the NC surface of a specific organic capping layer that would hinder the direct interaction either between the inorganic NCs with polymeric matrices or with other chemical environments.

The commonly accepted mechanism for tungsten oxide photochromism claims the formation of $\text{H}_x\text{W}^{6+}_{1-x}\text{W}^{5+}_x\text{O}_3$ is responsible for the blue color observed upon irradiation [27]. The combination with TiO₂ would clearly emphasize the coloration mechanism,

but to ensure an efficient and homogeneous photochromic behavior an intimate contact between TiO_2 and WO_{3-x} is a critical issue and, for that, high surface contact between both nanostructured building blocks needs to be guaranteed. The nanocrystalline colloids exhibit opposite surface charges (-39 mV for TiO_2 and $+2.8$ mV for WO_{3-x} related to Z-potential measurements performed on individual NC water solutions), which allows an electrostatic attraction between nanosized building blocks, and mutual interaction, therefore, when admixed in the same solution. When fabric samples were dipped into different NC solutions, the expressed photochromism reflects on photochromic textiles. Figure 2a reports a gallery of different pictures recorded on different samples impregnated with different $\text{WO}_{3-x}:\text{TiO}_2$ content (as reported by vertical annotations) and compared with only TiO_2 and WO_{3-x} impregnation. The relative elemental amounts were characterized and controlled by inductively coupled plasma optical emission spectrometry (ICP-OES, data not shown) to keep constant the overall inorganic amounts deposited on each textile. A first qualitative outcome of the different TiO_2 content on photochromic textiles can be appreciated with distinctive blue intensities obtained at different UV exposure times (as reported by horizontal annotations).

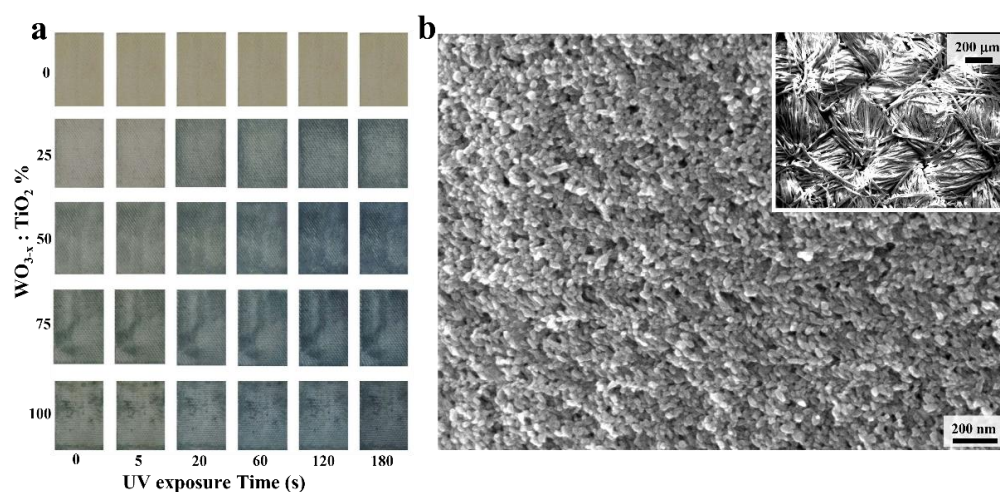


Figure 2. (a) Pictures recorded on textile samples functionalized via NC solution impregnation with different $\text{WO}_{3-x}:\text{TiO}_2$ contents; different degrees of blue are obtained with different UV exposure times for each composition. (b) Lower (inset) and higher magnification SEM micrograph of textiles functionalized with NC solution prepared with $\text{WO}_{3-x}:\text{TiO}_2$ ratio of 1:3 or 25%.

The nanostructured texture covering the pristine textile manufacture was characterized by SEM microscopy.

Figure 2b and Figure S1e report SEM images recorded on textile functionalized with NC solutions prepared with a $\text{WO}_{3-x}:\text{TiO}_2$ ratio of 25% after hotplate drying, without any other washing step. In particular, the inset of Figure 2b shows the fabric texture after NC impregnation and the higher magnification SEM images show complete and homogenous nanocrystalline coverage along the fibers (Figure 2b). In the Supporting Information, the SEM picture of one single fiber before and after NC impregnation is reported (Figure S1e,f). The pristine fiber is characterized by a fibrous motif/pattern (Figure S1f), which is not any more visible after impregnation (Figure S1e).

To investigate the photochromic textile performances with different $\text{WO}_{3-x}:\text{TiO}_2$ contents and compare them with two bare oxides on coloration and bleaching kinetics, detailed reflectance spectra were measured by a UV/Vis/NIR spectrometer. Figure 3a shows the reflectance changing values of NC-based photochromic fabrics of discrete compositions, at different UV exposure times and obtained at the two characteristic wavelengths of 550 nm and 830 nm. The individual reflectance spectra variations for each NC-functionalized photochromic fabric to different compositions are reported in Figure S2. The reflectance decreased within the initial 30 s and the changing rate became gradually slower with an

exponential trend, reaching a plateau (becoming saturated) within 5 min of UV exposure. It is worth underlying that a strong absorption in the IR and Vis regions already within 5 s of UV exposure was achieved only for the $\text{WO}_{3-x}:\text{TiO}_2$ mixture, compared with both pure oxide-coated textiles (TiO_2 alone does not show any photochromic behavior at the irradiate wavelength). The comparison of differences in reflectance between the no-exposure state and different times of UV exposure (ΔR) for all NC compositions are reported in Figure 3b (solid line for $\lambda = 550$ nm and dashed line for $\lambda = 830$ nm). It becomes clearer that the presence of TiO_2 increases the coloring kinetics for all mixture compositions compared with pure WO_{3-x} . Moreover, as the greatest ΔR values were achieved with a $\text{WO}_{3-x}:\text{TiO}_2$ ratio of 1:3 for both wavelengths, we selected this composition for further characterizations, as reported below. The after effect of TiO_2 blending (content) on the bleaching kinetics of the photochromic textiles was evaluated by monitoring, immediately after 5 min of UV exposure, the reflectance decay as a function of time. The representative reflectance values during the bleaching process of $\text{WO}_{3-x}:\text{TiO}_2$ functionalized textiles are reported in Figure 3c. All samples showed good reversible photochromic properties and TiO_2 blending was also revealed to be beneficial for photochromic recovery. Indeed, fabric samples containing TiO_2 blended with WO_{3-x} NCs showed a recovery of 80–100% (for $\lambda = 550$ nm) and 75–85% (for $\lambda = 830$ nm) values unlike samples functionalized with only WO_{3-x} , which recovered only the 75% and 70% of pristine reflectance values for Vis and IR, respectively (see Table 1 for specific values). All samples returned to their original bleached state after being stored in the dark (in the air) for about 6 h. Representative reflectance values are summarized in Table 1 for a more immediate comparison.

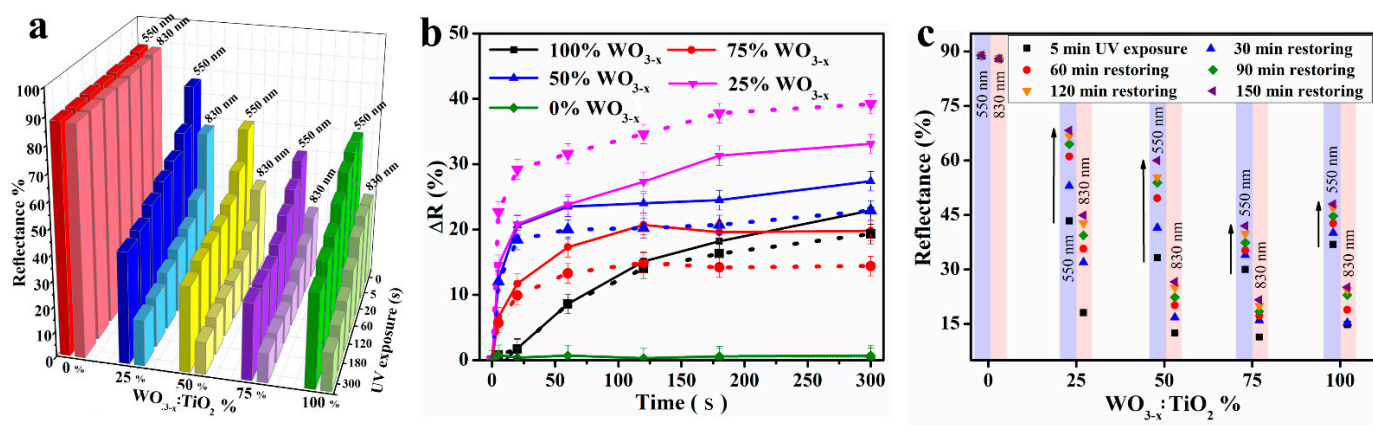


Figure 3. (a) Representative reflectance values at $\lambda = 550$ nm and $\lambda = 830$ nm of nanocrystalline-coated textile with different $\text{WO}_{3-x}:\text{TiO}_2$ compositions exposed to different UV irradiation times. (b) ΔR (difference between reflectance value after 5 min of UV exposure and no-exposed samples) variation at different UV exposure; solid lines are related to $\lambda = 550$ nm and dashed lines are related to $\lambda = 830$ nm. (c) Reflectance values during the bleaching process were carried out after 5 min of UV irradiation and recorded at different time intervals.

Table 1. $\text{WO}_{3-x}:\text{TiO}_2$ % related to different WO_{3-x} percentage content into NCs mixture for textile coating; $R_{\text{UV}=0}$ (550 nm) and $R_{\text{UV}=0}$ (830 nm) Reflectance percentage at 550 nm and 830 nm, respectively, of NC-functionalized samples with no UV exposure; $R_{\text{UV}=5 \text{ min}}$ (550 nm) and $R_{\text{UV}=5 \text{ min}}$ (830 nm) Reflectance percentage at 550 nm and 830 nm, respectively, of NC-functionalized samples with 5 min of UV exposure; $\Delta R_{550 \text{ nm}}$ and $\Delta R_{830 \text{ nm}}$ related to the difference between $R_{\text{UV}=5 \text{ min}}$ (550 nm)– $R_{\text{UV}=0}$ (550 nm) and $R_{\text{UV}=5 \text{ min}}$ (830 nm)– $R_{\text{UV}=0}$ (830 nm), respectively; R_{rec} (550 nm) and R_{rec} (830 nm) related to recovered reflectance percentage at 550 nm and 830 nm, respectively, of air-exposed samples kept 150 min in the dark; $\% \text{rec}_{(550 \text{ nm})}$ and $\% \text{rec}_{(830 \text{ nm})}$ related to percentage R_{rec} (550 nm) and R_{rec} (830 nm) compared to initial $R_{\text{UV}=0}$ (550 nm) and $R_{\text{UV}=0}$ (830 nm).

$\text{WO}_{3-x}:\text{TiO}_2$ %	$R_{\text{UV}=0}$ (550 nm)	$R_{\text{UV}=0}$ (830 nm)	$R_{\text{UV}=5 \text{ min}}$ (550 nm)	$R_{\text{UV}=5 \text{ min}}$ (830 nm)	$\Delta R_{550 \text{ nm}}$	$\Delta R_{830 \text{ nm}}$	R_{rec} (550 nm)	R_{rec} (830 nm)	$\% \text{rec}$ (550 nm)	$\% \text{rec}$ (830 nm)
0	88	88	88	88	0	0	0	0	-	-
25	75	55	42	15	33	40	68	45	90	82
50	60	35	34	15	26	20	60	28	100	80
75	50	25	30	12	20	13	40	21	80	84
100	60	33	38	15	22	18	47	25	78	75

The photochromic responses of the mixed oxide-functionalized textiles were tested in different alcoholic environments. Different photochromic responses or coloration intensities observed were compared in Figure 4a, while individual reflectance spectra variation recorded on 25% WO_{3-x} impregnated textiles soaked with different solvents were reported in Figure S3. For that aim, we selected the textile sample functionalized with $\text{WO}_{3-x}:\text{TiO}_2$ (25% WO_{3-x}) because of its greater ΔR observed without any additive. We monitored the reflectance as a function of UV time exposure after soaking each sample with 300 μL of selected organic solvent (see experimental details). The largest optical response in the Vis as well as in the NIR was achieved with MeOH, followed by EtOH and i-PrOH, which show also an improvement in coloration sensitivity for both wavelengths compared with pristine samples (NC-coated textile with no alcohol impregnation) (Figure 4b). Moreover, we used acetone for comparison which did not show any coloration improvement (data not shown). Our interpretation of the increased modulation relates to the protic nature of alcohols compared with the aprotic habit of acetone, while the observed modulation trend (MeOH > EtOH ~ i-PrOH) could be attributed to the greater acidity of MeOH compared with EtOH and i-PrOH (pKa MeOH ~ 15.5; pKa EtOH ~ 16; pKa i-PrOH ~ 17) or to their intrinsic hole scavenger nature (see Discussion below for a more exhaustive analysis).

Based upon this solvent effect, the following measurements were conducted with a suitable polymeric medium in order to mimic the solvent behavior in a solid-state. As the presence of hydroxyl groups increases the photochromic efficiency [28] we selected hydroxyl-rich, cheap, non-toxic, and naturally abundant materials as a polymeric matrix. For this purpose we over-coated the NC-functionalized textile with two alternative polysaccharides, taking advantage of structural –OH moieties present in their chemical structures. More specifically, we compared corn starch and hydroxyethylcellulose (HEC). Both of them underwent a gelation process (rather than a full dissolution) when stirred in hot (80 °C) water, while they became badly water-soluble at room temperature, materials suitable in view of greener chemistry since no organic solvents were adopted for polymer overcoating. It is worth saying that HEC displays easier solubility and processability at higher concentrations, which is a not negligible detail in the view of the industrial scalability process. Pictures of different photochromic responses recorded on as described samples are reported in Figure 4a. The reflectance variations as a function of UV exposure times are compared in Figure 4b, while individual reflectance spectra variation recorded on 25% WO_{3-x} -impregnated textiles over-coated with different polymers are reported in Figure S4. The HEC-coated photochromic textile reported faster and stronger exponential modulation sensitivity than pristine samples as well as compared with EtOH and i-PrOH soaked samples, while slightly reduced compared with MeOH both in the Vis and NIR window with comparable UV exposure time. The starch-coated photochromic textile re-

ported similar behavior as the EtOH and *i*-PrOH treated textiles. The bleaching kinetics, reported in Figure 4c, remain mainly influenced by the TiO₂ presence in the inorganic NCs blend and was not substantially inferred by any further over-coating, besides Nafion (see below). To investigate the coloring–bleaching cycles stability, specific experiments were carried out with the HEC over-coated WO_{3-x}:TiO₂ (25%) textile, by exposing a sample to repeated cycles of 5 min UV irradiation and then keeping it at 75 °C under air on a hot plate to accelerate the bleaching condition. We stressed the sample with 100 cycles and the results are reported in Figure 4d. The initial reflectance (in the colored state) of each cycle raises by increasing the number of irradiation cycles, ascribable this to a little decline in photochromism. For comparison, we over-coated the NC-functionalized textile with Nafion. Samples reported an extremely fast and intense, though irreversible, modulation for Vis ($\lambda = 550$) and NIR ($\lambda = 830$) wavelengths. We suppose this to be due to the intrinsic high acidity of sulfonic moieties in the Nafion chemical structure, which could stabilize the chemical structure responsible for the colored state.

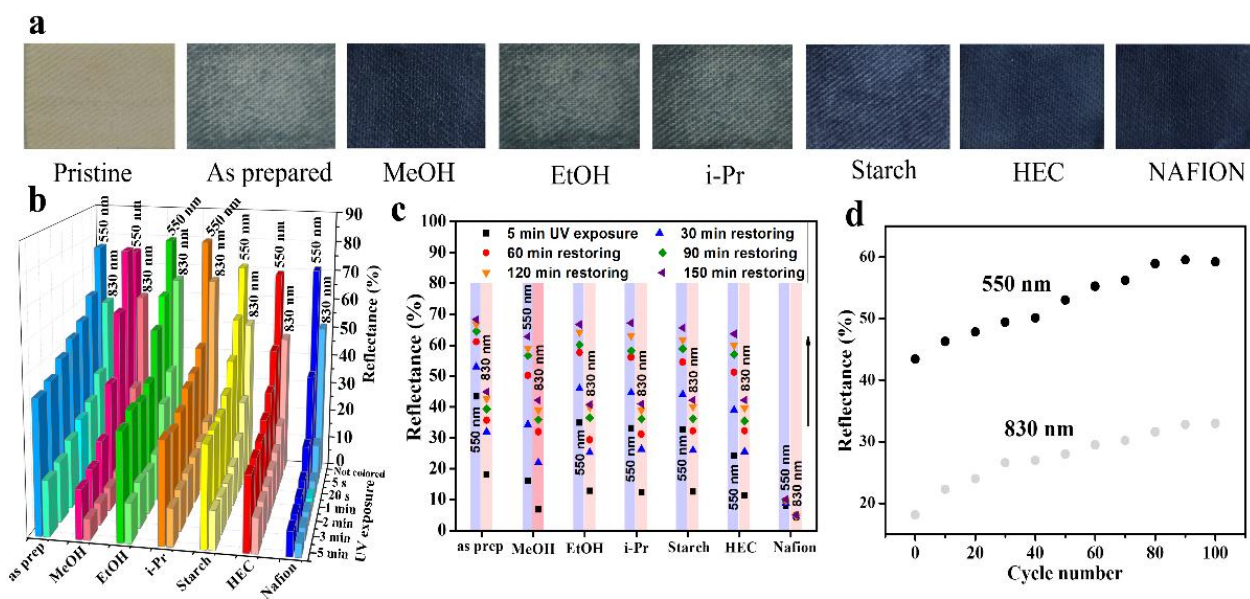


Figure 4. (a) Pictures of soaked or over-coated textile sample previously functionalized with NC solution of WO_{3-x}:TiO₂ (25% WO_{3-x}) and UV irradiated for 5 min. (b) Representative reflectance values during coloring process with different UV exposure and (c) and bleaching process carried out after 5 min of UV irradiation and recorded at different time intervals for $\lambda = 550$ nm and $\lambda = 830$ nm on soaked or over-coated textile's sample previously functionalized with NC solution containing WO_{3-x}:TiO₂ (1:3). (d) Cycling property of HEC over-coated WO_{3-x}:TiO₂ (25% WO_{3-x}) textile exposed to 100 cycles of 5 min UV irradiation followed by 5 min heated at 75 °C.

Contact angle measurements were performed to evaluate functionalized fabrics' wettability (Figure S5). All functionalized fabrics (except the one treated with Nafion) showed high wettability and the water drops were rapidly adsorbed within a few hundred ms. For this reason, it was not possible to evaluate the contact angle. In the case of fabrics coated with starch and HEC, the hydrophilic nature of the two polymers led to an absorption of the drop in times very similar to those of the pristine fabric. In the case of fabrics treated with nanocrystals only (100% TiO₂ or 100% WO_{3-x}), the adsorption of the drop is even faster, occurring in less than 100 ms. Only fabric coated with Nafion, a fluorinated polymer, acquired good hydrophobicity, with slightly asymmetrical left–right contact angles due to the surface morphology of the fabric (113° left, 120° right).

To demonstrate the proof of concept of a free-standing membrane, a prototype was fabricated following the identical experimental procedures described in this study. For that, WO_{3-x} and TiO₂ solutions (25% WO_{3-x}) were dispersed in an HEC solution (50 mg/mL),

cast onto a hydrophobic substrate, and then dried at 70 °C for 2 h. The as-deposited film could be detached from the substrate and used as a free-standing photochromic membrane. This lab-scale prototype has a dimension of about 3 cm × 3 cm and shows a good color change modulation. Pictures of the bleached and colored states are shown in Figure 5. This represented just a proof of concept for developing a sticky photochromic membrane to be eventually attached and detached onto any kind of already fabricated textiles.

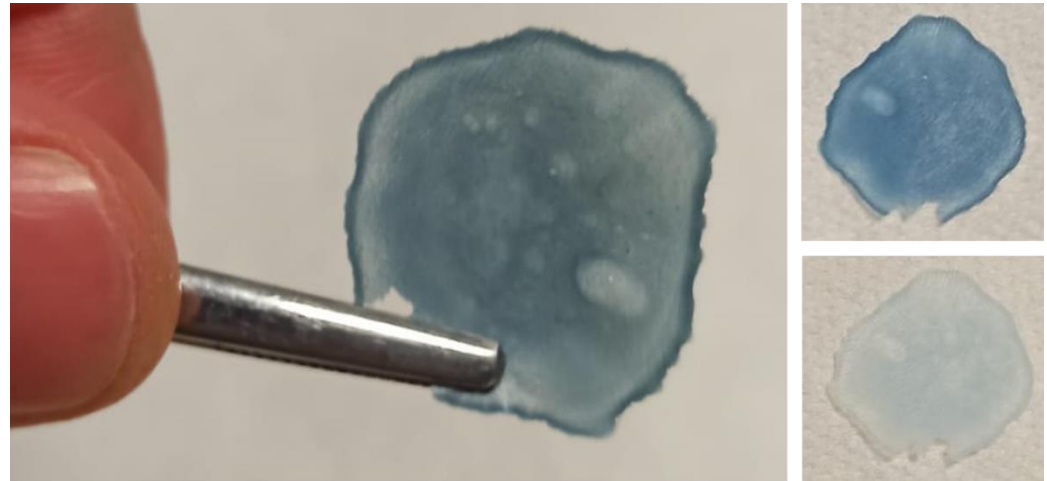
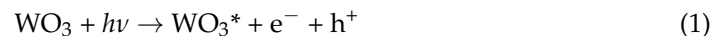


Figure 5. Pictures of photochromic freestanding membrane both in bleached and colored states.

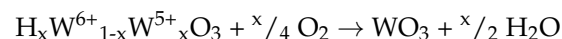
4. Discussion

The commonly accepted photo-induced coloration mechanism for tungsten oxide, which represents the photo-active optical material for our purpose, can be roughly summarized as follows:

Coloration process:



Bleaching process:



The irradiation of WO_3 with UV-light induces the excitation of electrons to the conduction band and the formation of holes in the valence band (Reaction 1). The photogenerated holes can interact with absorbed water molecules, thus inducing the decomposition into protons and oxygen radicals (Reaction 2). Finally, photogenerated electrons react with protons and WO_3 with the formation of hydrogen tungsten bronze responsible for the blue color (Reaction 3).

In comparison with pure WO_3 (as well as for its substoichiometric counterpart WO_{3-x}), as for other reported oxide samples such as MoO_3 (into CdS/WO_3 bi-layers and for $\text{MoO}_3/\text{TiO}_2$ composites), the suddenly reported photochromic mechanism for WO_3 is maximized by the presence of TiO_2 . Thus, $\text{WO}_{3-x}:\text{TiO}_2$ blends exhibited much stronger photochromic properties to date, an effect mainly ascribable to hetero-interface formation between the two oxides [28,36]. WO_{3-x} and TiO_2 are both n-type semiconductors and can both be excited by UV light, generating holes and electrons (reaction 1). Because of the staggered alignment of the energetics bands, the photogenerated holes can be transferred from the WO_{3-x} valence band to the TiO_2 valence band and the electrons can transfer from the TiO_2 conduction band to the WO_{3-x} conduction band. The segregation of photoexcited carriers into two different materials would consequently increase the electron-hole lifetime.

The photo-produced hole can weaken the H–O bond of adsorbed water molecules, or other H-O-containing species, and causes the water molecules decomposition into a proton and highly reactive oxygen radicals (reaction 2). While protons diffuse into the lattice, the photogenerated electrons injected into the conduction band of WO_{3-x} , balanced by proper counterions (i.e., protons), react inducing the reduction of W(VI) to W(V) and generate $\text{H}_x\text{W}^{6+}_{1-x}\text{W}^{5+}_x\text{O}_3$, (hydrogen tungsten bronze) (reaction 3). Moreover, it was suggested that the coloration in WO_{3-x} could also be due to electrons trapped at energy levels within the forbidden gap, which can lead to a broad absorption in the IR region when they are excited into higher energy levels [28]. A representative scheme of photochromism in the $\text{WO}_{3-x}:\text{TiO}_2$ systems is shown in Figure 6.

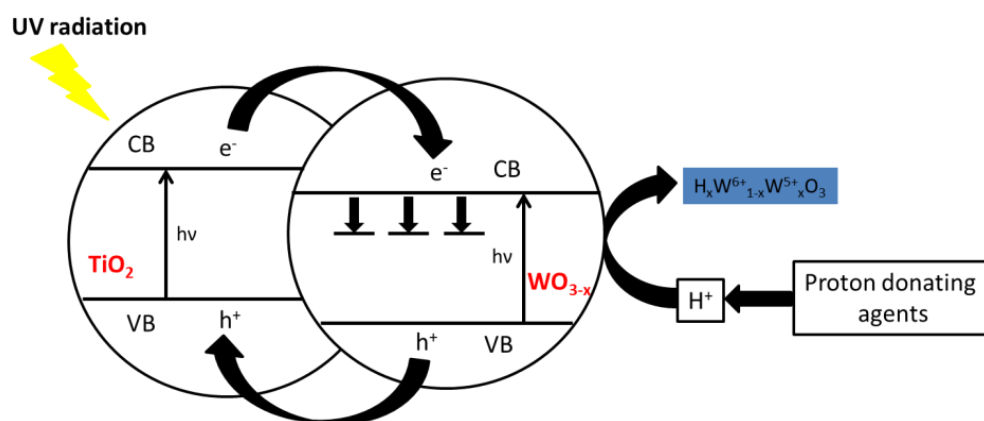


Figure 6. Scheme of photochromism mechanism in $\text{WO}_{3-x}:\text{TiO}_2$ systems.

Therefore, the photogenerated carriers in $\text{WO}_{3-x}:\text{TiO}_2$ blends are more effectively separated with respect to pure WO_3 and result in improved coloration performances because of the effective interfacial interaction. In particular, the more protons diffuse into the lattice, the more hydrogen tungsten bronze will be formed, and faster and stronger polaronic absorption will be obtained.

The number of available protons depends on the amount and nature of the surface adsorbed solvents such as H_2O , or alcohols. Alcohol can form protons easier because of its greater proton acidity compared to water, therefore, $\text{WO}_{3-x}:\text{TiO}_2$ alcohol-wetted fabrics showed larger photochromic efficiency than as-prepared samples (i.e., only NC-functionalized) where the photochromism is most probably powered by atmospheric water [35]. Moreover, alcohols (particularly MEOH) are largely used in photocatalytic similar systems for their prerogative of acting as an efficient hole scavenger or, in other words, used as a sacrificial electron donor for the depletion of photogenerated holes, thus they would partially inhibit intrinsic charges quenching.

Therefore, methanol represents the best solvent for improving the performance of the photochromic fabrics, both in terms of acidity and hole scavenger properties.

The nanoscale dimensions of inorganic colloids play also a fundamental role for two main reasons: (i) they decrease the distance of charges transfer, thus increasing the rate of coloration and decreasing the time of de-coloration; (ii) they maximize the surface-assisted hetero-interface interaction between oxides contributing to the higher charge transfer and ion intercalation kinetics, favoring the overall photochromic efficiency.

In the examples of over-coating with polymeric matrices, the –OH moieties in their chemical structure can enhance the number of available protons thus inducing an improvement of photochromic performances (as observed for alcohol impregnated samples), while the polymeric chain and the presence of hydrogen bonds would facilitate the migration of produced H^+ and electrons.

Polymers with this prerogative, with an adequate viscosity that would guarantee enough ionic mobility and eventually could show interesting foil-forming potential, would

be of great interest for accelerating coloration and bleaching behavior of the tungsten oxide-based hybrid photochromic foil with outstanding cycling stability.

5. Conclusions

In this work, photo-sensitive chromogenic smart textiles were realized with a straightforward industrially practicable approach potentially extendible over a broad range of every hydrophilic fabric. For that, commercial fabrics were functionalized with mixtures of WO_{3-x} and TiO_2 nanocrystalline breeds to produce photochromic textiles. Because of nanometric particle size and their peculiar opposite surface charges, high specific surface areas with rich interfacial sites for charge transfer were created and hetero-interfaces were designed through strong electrostatic interactions. Indeed, an enhanced and reversible optical response both in the visible ($\lambda = 550$ nm) and infrared ($\lambda = 830$ nm) ranges was obtained. Moreover, the photochromic behaviors of nano-functionalized textiles exposed to different solvents and dispersed in several matrices were studied. Analyses of the different coloring and bleaching efficiencies were performed to reach an optimal balance between coloration and discoloration behavior along with consistent cycling stability. Furthermore, by using hydroxyl-rich water-dispersible polysaccharides over-coating the nano-functionalized textiles, an interesting enhancement of the overall photochromic response was generated. Those substrates furnish non-toxic, unpolluted, moldable rigidity, strong adhesion, and solvent resistance platforms for different practical useful textile applications or even photochromic freestanding foils. The high UV sensitivity and the filmogenic nature of the resulting hybrid materials make them important candidates for application in practical UV sensing devices and light-activated smart textiles.

Supplementary Materials: The following supporting information can be downloaded at: <https://www.mdpi.com/article/10.3390/textiles2030021/s1>, Figure S1: TEM, SEM images and XRD diffraction pattern. Figure S2: Reflectance spectra of NCs impregnated textiles in the bleached state and for different UV irradiation times. Figure S3: Reflectance spectra of $\text{WO}_{3-x}:\text{TiO}_2$ (1:3) (25% WO_{3-x}) impregnated textiles soaked with different solvents. Figure S4: Reflectance spectra of $\text{WO}_{3-x}:\text{TiO}_2$ (1:3) (25% WO_{3-x}) impregnated textiles over-coated with different polymeric matrices. Figure S5. Contact angle measurements on functionalized fabrics.

Author Contributions: Conceptualization: R.S., M.P. and R.G. Methodology: R.S., V.P., S.C., and C.D.V. Software: F.M. and A.M. Formal analysis: R.S. and V.P.; Investigation, Data curation, Writing—original draft preparation: R.S. Reviewing: L.C. and C.T.P. Editing: R.S. Founding acquisition: V.M. All authors have read and agreed to the published version of the manuscript.

Funding: This research was funded by “ECO-sustainable and intelligent fibers and fabrics for TECHnic clothing (ECOTECH)”, PON «R&I» 2014–2020, project N° ARS01_00951, CUP B66C18000300005—COR 577006, Azione II—OS 1.b—D.D. Prot. N. 2055 del 02/08/2018.

Data Availability Statement: The data presented in this study are available on request from the corresponding author.

Acknowledgments: The authors appreciate the technical support and fabrics provided by Klopman Srl.

Conflicts of Interest: The authors declare no conflict of interest.

References

1. Stoppa, M.; Chiolerio, A. Wearable Electronics and Smart Textiles: A Critical Review. *Sensors* **2014**, *14*, 11957–11992. [[CrossRef](#)] [[PubMed](#)]
2. Shah, M.A.; Pirzada, B.M.; Price, G.; Shibiru, A.L.; Qurashi, A. Applications of Nanotechnology in Smart Textile Industry: A Critical Review. *J. Adv. Res.* **2022**, *38*, 55–75. [[CrossRef](#)] [[PubMed](#)]
3. Cinquino, M.; Prontera, C.; Pugliese, M.; Giannuzzi, R.; Taurino, D.; Gigli, G.; Maiorano, V. Light-Emitting Textiles: Device Architectures, Working Principles, and Applications. *Micromachines* **2021**, *12*, 652. [[CrossRef](#)] [[PubMed](#)]
4. Ojha, G.P.; Pant, B.; Acharya, J.; Park, M. Prussian Red Anions Immobilized Freestanding Three-Dimensional Porous Carbonaceous Networks: A New Avenue to Attain Capacitor- and Faradic-Type Electrodes in a Single Frame for 2.0 v Hybrid Supercapacitors. *ACS Sustain. Chem. Eng.* **2022**, *10*, 2994–3006. [[CrossRef](#)]

5. Pant, B.; Ojha, G.P.; Kuk, Y.S.; Kwon, O.H.; Wan Park, Y.; Park, M. Synthesis and Characterization of ZnO-TiO₂/Carbon Fiber Composite with Enhanced Photocatalytic Properties. *Nanomaterials* **2021**, *11*, 960. [[CrossRef](#)]
6. Dang, T.; Zhao, M. The Application of Smart Fibers and Smart Textiles. *J. Phys. Conf. Ser.* **2021**, *1790*, 12084. [[CrossRef](#)]
7. Ferrara, M.; Bengisu, M. *Materials That Change Color: Smart Materials, Intelligent Design*; Springer Briefs in Applied Sciences and Technology; Springer: Cham, Switzerland, 2013; ISBN 3319002899.
8. Khattab, T.A.; Rehan, M.; Hamouda, T. Smart Textile Framework: Photochromic and Fluorescent Cellulosic Fabric Printed by Strontium Aluminate Pigment. *Carbohydr. Polym.* **2018**, *195*, 143–152. [[CrossRef](#)]
9. Bashari, A.; Shakeri, M.; Shirvan, A.R. *UV-Protective Textiles*; Elsevier Ltd.: Amsterdam, The Netherlands, 2018; ISBN 9780081024911.
10. Karpagam, K.R.; Saranya, K.S.; Gopinathan, J.; Bhattacharyya, A. Development of Smart Clothing for Military Applications Using Thermochromic Colorants. *J. Text. Inst.* **2017**, *108*, 1122–1127. [[CrossRef](#)]
11. Seipel, S.; Yu, J.; Viková, M.; Vik, M.; Koldinská, M.; Havelka, A.; Nierstrasz, V.A. Color Performance, Durability and Handle of Inkjet-Printed and UV-Cured Photochromic Textiles for Multi-Colored Applications. *Fibers Polym.* **2019**, *20*, 1424–1435. [[CrossRef](#)]
12. Seipel, S.; Yu, J.; Periyasamy, A.P.; Viková, M.; Vik, M.; Nierstrasz, V.A. Inkjet Printing and UV-LED Curing of Photochromic Dyes for Functional and Smart Textile Applications. *RSC Adv.* **2018**, *8*, 28395–28404. [[CrossRef](#)]
13. Wu, S.; Fan, J.; Wang, W.; Yu, D. Smart Screen-Printed Photochromic Fabrics with Fast Color Switching Performance and High Fatigue Resistance for Energy Storage Applications. *Colloids Surf. A Physicochem. Eng. Asp.* **2022**, *632*, 127760. [[CrossRef](#)]
14. Zheng, Y.; Panatdasirisuk, W.; Liu, J.; Tong, A.; Xiang, Y.; Yang, S. Patterned, Wearable UV Indicators from Electrospun Photochromic Fibers and Yarns. *Adv. Mater. Technol.* **2020**, *5*, 2000564. [[CrossRef](#)]
15. He, Z.; Wang, W.; Fan, J.; Bao, B.; Qin, X.; Yu, D. Photochromic Microcapsules Anchored on Cotton Fabric by Layer-by-Layer Self-Assembly Method with Erasable Property. *React. Funct. Polym.* **2020**, *157*, 104762. [[CrossRef](#)]
16. Abate, M.T.; Seipel, S.; Yu, J.; Viková, M.; Vik, M.; Ferri, A.; Guan, J.; Chen, G.; Nierstrasz, V. Supercritical CO₂ Dyeing of Polyester Fabric with Photochromic Dyes to Fabricate UV Sensing Smart Textiles. *Dye. Pigment.* **2020**, *183*, 108671. [[CrossRef](#)]
17. Billah, S.M.R.; Christie, R.M.; Shamey, R. Direct Coloration of Textiles with Photochromic Dyes. Part 3: Dyeing of Wool with Photochromic Acid Dyes. *Color. Technol.* **2012**, *128*, 488–492. [[CrossRef](#)]
18. He, Z.; Bao, B.; Fan, J.; Wang, W.; Yu, D. Photochromic Cotton Fabric Based on Microcapsule Technology with Anti-Fouling Properties. *Colloids Surf. A Physicochem. Eng. Asp.* **2020**, *594*, 124661. [[CrossRef](#)]
19. Liu, X.; Cheng, T.; Parhizkar, M.; Wang, X.; Lin, T. Photochromic Textiles from Hybrid Silica Coating with Improved Photostability. *Res. J. Text. Appar.* **2010**, *14*, 1–8. [[CrossRef](#)]
20. Parhizkar, M.; Zhao, Y.; Wang, X.; Lin, T. Photostability and Durability Properties of Photochromic Organosilica Coating on Fabric. *J. Eng. Fibers Fabr.* **2014**, *9*, 155892501400900320. [[CrossRef](#)]
21. Pinto, T.V.; Costa, P.; Sousa, C.M.; Sousa, C.A.D.; Pereira, C.; Silva, C.J.S.M.; Pereira, M.F.R.; Coelho, P.J.; Freire, C. Screen-Printed Photochromic Textiles through New Inks Based on SiO₂@naphthopyran Nanoparticles. *ACS Appl. Mater. Interfaces* **2016**, *8*, 28935–28945. [[CrossRef](#)]
22. Ling, Z.; Liu, K.; Zou, Q.; Li, Q.; Zhang, K.-Q.; Cui, Z.; Yuan, W.; Liu, Y. Continuous and Rapid Fabrication of Photochromic Fibers by Facilely Coating Tungsten Oxide/Polyvinyl Alcohol Composites. *RSC Adv.* **2018**, *8*, 28581–28587. [[CrossRef](#)]
23. Wang, X.; Wang, W.; Li, Y.; Wang, Y. Preparation of Tungsten-Based Polyvinyl Alcohol Waterborne Coating and Development of Photochromic Composite Fabric. *Macromol. Mater. Eng.* **2021**, *306*, 2100540. [[CrossRef](#)]
24. Fang, W.; Sairanen, E.; Vuori, S.; Rissanen, M.; Norrbo, I.; Lastusaari, M.; Sixta, H. UV-Sensing Cellulose Fibers Manufactured by Direct Incorporation of Photochromic Minerals. *ACS Sustain. Chem. Eng.* **2021**, *9*, 16338–16346. [[CrossRef](#)]
25. Bao, B.; Fan, J.; Wang, Z.; Wang, Y.; Wang, W.; Qin, X.; Yu, D. Sodium Deca-Tungstate/Polyacrylic Acid Self-Assembled Flexible Wearable Photochromic Composite Fabric for Solar UV Detector. *Compos. Part B Eng.* **2020**, *202*, 108464. [[CrossRef](#)]
26. Wei, J.; Jiao, X.; Wang, T.; Chen, D. Electrospun Photochromic Hybrid Membranes for Flexible Rewritable Media. *ACS Appl. Mater. Interfaces* **2016**, *8*, 29713–29720. [[CrossRef](#)] [[PubMed](#)]
27. He, T.; Yao, J.N. Photochromism in Transition-Metal Oxides. *Res. Chem. Intermed.* **2004**, *30*, 459–488. [[CrossRef](#)]
28. He, T.; Yao, J. Photochromism in Composite and Hybrid Materials Based on Transition-Metal Oxides and Polyoxometalates. *Prog. Mater. Sci.* **2006**, *51*, 810–879. [[CrossRef](#)]
29. He, T.; Ma, Y.; Cao, Y.; Hu, X.; Liu, H.; Zhang, G.; Yang, W.; Yao, J. Photochromism of WO₃ Colloids Combined with TiO₂ Nanoparticles. *J. Phys. Chem. B* **2002**, *106*, 12670–12676. [[CrossRef](#)]
30. Li, H.; Wu, H.; Xiao, J.; Su, Y.; Robichaud, J.; Brüning, R.; Djaoued, Y. A Hierarchically Porous Anatase TiO₂ Coated-WO₃ 2D IO Bilayer Film and Its Photochromic Properties. *Chem. Commun.* **2016**, *52*, 892–895. [[CrossRef](#)]
31. Radhika, T.; Ramalingam, R.J.; Aneesa, V.; Albaqami, M.D. Synthesis and Characterization of Photochromic Inkless Coating Based on WO₃-Titania Nanocomposite under Sun Light and Solar Simulation Condition. *Optik* **2021**, *228*, 166145. [[CrossRef](#)]
32. Djaoued, Y.; Balaji, S.; Beaudoin, N. Sol-Gel Synthesis of Mesoporous WO₃-TiO₂ Composite Thin Films for Photochromic Devices. *J. Sol-Gel Sci. Technol.* **2013**, *65*, 374–383. [[CrossRef](#)]
33. Li, R.; Zhou, Y.; Shao, Z.; Zhao, S.; Chang, T.; Huang, A.; Li, N.; Ji, S.; Jin, P. Enhanced Coloration/Bleaching Photochromic Performance of WO₃ Based on PVP/PU Composite Matrix. *ChemistrySelect* **2019**, *4*, 9817–9821. [[CrossRef](#)]

34. Scarfiello, R.; Prontera, C.T.; Pugliese, M.; Bianco, G.V.; Bruno, G.; Nobile, C.; Carallo, S.; Fiore, A.; Sibillano, T.; Giannini, C.; et al. Electrochromic Evaluation of Airbrushed Water-Dispersible $W_{18}O_{49}$ Nanorods Obtained by Microwave-Assisted Synthesis. *Nanotechnology* **2021**, *32*, 215709. [[CrossRef](#)] [[PubMed](#)]
35. Yao, J.N.; Loo, B.H.; Hashimoto, K.; Fujishima, A. Photochromic Characteristics of Mixed WO_3 - MoO_3 Thin Films in Alcohol Vapors. *Ber. Der Bunsenges. Für Phys. Chem.* **1991**, *95*, 554–556. [[CrossRef](#)]
36. Tatsuma, T.; Saitoh, S.; Ngaotranwiwat, P.; Ohko, Y.; Fujishima, A. Energy Storage of TiO_2 - WO_3 Photocatalysis Systems in the Gas Phase. *Langmuir* **2002**, *18*, 7777–7779. [[CrossRef](#)]